ANBALAGAN, A., ARUMUGAM, E. and MICHAEL, A.X. 2021. A FEA simulation study of ball end mill for fixed 3+1 / 3+2 axis machining of Ti-6Al-4V. Materials today: proceedings [online], 46(17): proceedings of 3rd International conference on materials, manufacturing and modelling 2021 (ICMMM 2021), 19-21 March 2021, [virtual conference], pages 7803-7814. Available from: https://doi.org/10.1016/j.matpr.2021.02.369

A FEA simulation study of ball end mill for fixed 3+1 / 3+2 axis machining of Ti-6Al-4V.

ANBALAGAN, A., ARUMUGAM, E. and MICHAEL, A.X.

2021

Available online at www.sciencedirect.com

ScienceDirect

materialstoday: PROCEEDINGS

[ICMMM 2021]

A FEA Simulation Study of Ball End Mill for Fixed 3+1/3+2 Axis Machining of Ti-6Al-4V

Arivazhagan Anbalagan[a] , Eakambaram Arumugam[b] , M Anthony Xavior[c]

[a]*School of Engineering, Robert Gordon University, Garthdee House, Garthdee Road, Aberdeen, AB10 7QB, Scotland, UK,*
[b]*School of Mechanical Engineering, Arunai Engineering College, Tiruvannamalai, - 606 603, Tamilnadu, INDIA,*
[c]*Department of Manufacturing Engineering, School of Mechanical Engineering, VIT University, Vellore – 632014, Tamil Nadu, INDIA.*

Abstract

This paper presents a Finite Element Analysis (FEA) simulation study conducted on ball endmill for fixed 3+1 and 3+2 axis orientations for machining Ti-6Al-4V. This work adopts a tungsten carbide (WC) Ø18.6mm diametrical / 6fluted ball endmill to analyse maximum principal elastic strain ($\varepsilon_{max\text{-}max\text{-}principal\text{-}elastic}$), maximum principal stress ($\sigma_{max\text{-}principal}$) along with cutting tools forces in the axial (F_z), radial (F_y), tangential (F_x) and total (F_{total}) directions. The machining orientations considered for 3+1 and 3+2 axis are (i) tilt angles of 5°, 10°, 15° & 20° and (ii) lead angles of 5°, 10° & 15° with a constant fixed tilt angle of 10°. The cutting speed and feed rate per tooth is taken as 450m/min and 0.5 mm/tooth. These are based on a high speed machining (HSM) scenario and has been dynamically simulated for a maximum of 175,000 cycles. From the simulation study considered at 16-20 valid cutting points, it can be noticed that in 3+1 axis, for a tilt angle of 10° and 3+2 axis for a Tilt 10°/Lead 10° the $\sigma_{max\text{-}principal}$ and $\varepsilon_{max\text{-}max\text{-}principal\text{-}elastic}$ are higher when compared with all tilt/lead angles. In case of total forces (F_{total}) from all 3 directions (F_x, F_y and F_z) not much variation can be noticed for different tilt / lead angles, but higher values are recorded with 3+1 axis at 5° tilt angle and 3+2 axis at tilt/lead angle of 10°. The paper provides a critical comparative study on the 3+1/ 3+2 axis orientations highlighting the cutting strain/stress with tool forces at valid cutting points considering entry, middle and exit region of the blank by emphasizing the importance of cutting tool design parameters.

Keywords: 3+1 / 3+2 axis, Ti-6Al-4V, Tilt / Lead angle, Finite Element Analysis, Machining, Tool Forces, Stresses & Strains.

1. Introduction and Literature Review

Machining of Ti-6Al-4V based free form parts involving Bezier or B-Spline surfaces requires varying axis orientations at different locations of features because of its associated complexity and importance [1-5]. Mostly, at different cross sections, these parts are initially rough machined in a 3-axis, followed by semi finishing/ partial finishing with fixed 3+1 / 3+2 axis and finishing them with a full 5 axis operation. Specifically, in machining of die and injection moulds made of Ti-6Al-4V seen in aerospace / automobile / oil & gas domains, 85-90% of the machining operations including roughing/semi finishing are run with the fixed 3+1 / 3+2 axes giving 3 and 5 axis within a 15-10% range of usage [1-2]. The reason is by using a 3+1/3+2 setup a workpiece can be machined from all sides reducing the need for additional set ups thereby lowering the cycle time and reducing costs. 3+1/3+2 axes can also use a shorter, more rigid cutting tool than a regular three-axis machining, resulting in greater dimensional stability [4]. Fig.1 shows the schematic representation to achieve various axis orientations in a CNC machine [2-4]. Here 'A' 'B' and 'C' are tool rotation orientations constituting the 4th and 5th axis either through the table or spindle head. Despite the advantages of 3+1/3+2 axes, in any case, the life of tool, associated wear, surface roughness and tolerance remains a challenge as full cutting edge/face will not be engaged like a 3-axis machining. In other terms, the cutting tool will engage with varied rake/relief angle increasing the chance of generating internal stresses and strains. As shown in the Fig.2(a-f), in a fixed 3+1/3+2 axis the tool orientation is stationary, but many times slight change with the movement

of the tool to machine Ti-6Al-4V with internals slots i.e. undercut/ over cuts requires care full consideration while machining [2-5]. Moreover, the depth associated in these shapes, and the neck length plays a major role in movements and with the machining of these components [5]. Because of this, many times tool breakages will be encountered damaging the workpiece (like small chippings, dents etc) giving rise to frequent cutting tool replacement by the process planner / machinist and thereby increasing total machining time / cost. This is possible despite being ability of most sophisticated CAD/CAM software's to identify the collisions during the toolpath generation, and even after a rigorous check for collisions with both tool to work piece / fixture by Computer Aided Design / Computer Aided Manufacturing (CAD/CAM) engineers. One reason is, during the toolpath generation and validation, material aspects are not considered at these locations as material-based toolpath generation and validation remains an open challenge. In the present Industry 4.0 era [6-7], digital geometry-based simulations are the best way to achieve a digital twin like technology using various Internet of Technologies (IoT) concepts [7] by analysing the tool and work blank interactions/ contacts and to determine the chance of tool breakages, identifying stresses/strains and forces associated with the machining. But this open problem is still under development and may require time to accomplish a parallel prediction.

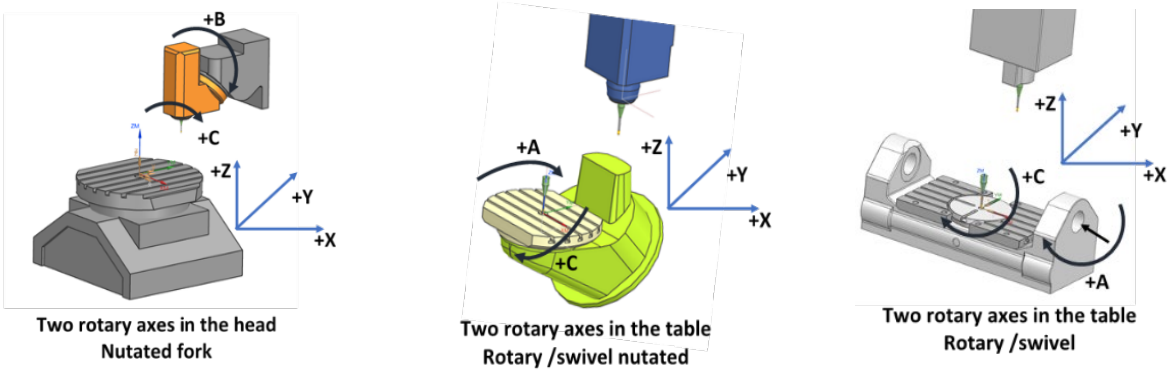

Fig. 1. Various 3+1/3+2 axis orientations in CNC machines either through the table or spindle head.

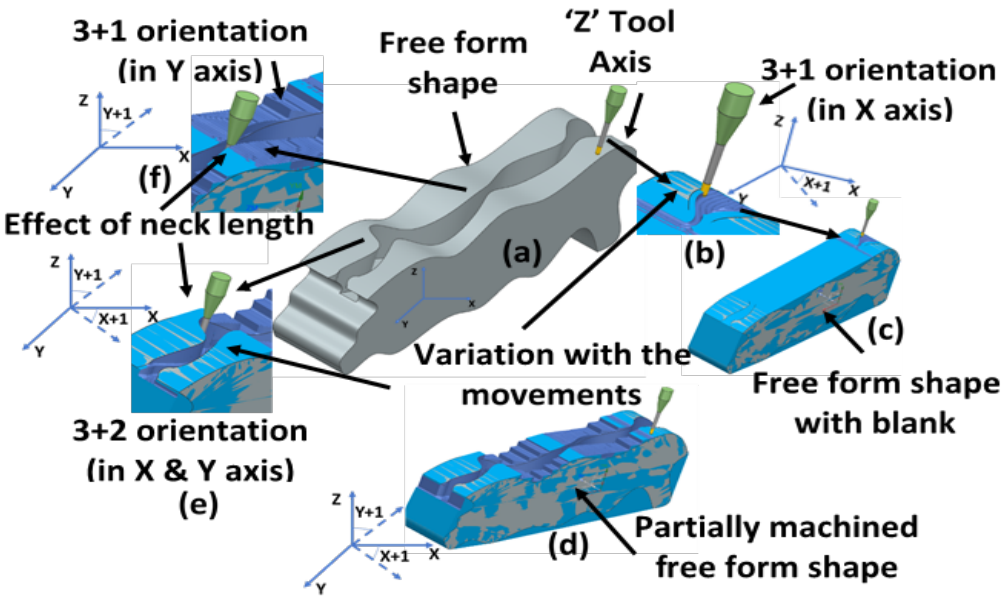

Fig. 2. Possible tool orientations in 3+1/3+2 axis (fixed) while machining free form shapes / features

The immediate solution as known and handled by many researchers is the use of Finite Element Analysis (FEA) analysis [8-15] by developing digital geometry of the cutting tool and blank to determine the stresses ($\sigma_{max/min\text{-}principal}$), strains ($\varepsilon_{max/min(elastic\ and\ equivalent\ plastic/elastic)}$) and the forces (F) in the axial (F_z), radial (F_y), tangential (F_x) and total (F_{total}) directions [10, 12, 15, 18, 21]. By carefully analysing the cutting tool design and the associated dimensional parameters like rake angles, relief angles issues like tool chatter and vibrations [17] leading to cutter runout and fixture

movement can be eliminated. Generally, the Ti-6Al-4V parts are machined in a high speed machining (HSM) environment with higher speeds / feeds, spindle rotations where FEA simulation before machining of these crucial components will be helpful to predict the parameters are mentioned above. Thanongsak Thepsonthi, Tugrul Özel [8] presented a 3-D FE based process simulations on micro-end milling of titanium alloy Ti-6Al-4V with uncoated WC/Co micro-end mills. The work has been conducted in DEFORM 3-D software where they analysed and verified the experimentally the simulated chip width, the cutting force components (Fx, Fy, and Fz), temperature and tool wear. Puneet Tandon & Md. Rajik Khan [9] proposed a methodology to design a CAD model of flat end mill and to perform FEA analysis for a four-fluted M42 High Speed Steel. It is by static and transient dynamic analysis to validate the structural integrity and verifying the stress distribution, deformation, and displacement. Xiaoliang Jin & Yusuf Altintas [10] modelled orthogonal micro-cutting process by considering the chip size and tool edge radius effect and predicted the micro-milling forces including the tool trajectory, tool run-out and dynamometer dynamics. The work considers a FE model to compare against the slip-line field simulation and turning experimental results to predict the milling forces by adjusting the cutting force coefficients.

A FEM simulation for shoulder milling operations for 304L stainless steel is presented by A. Maurel-Pantel et.al [11]. In the work an explicit solution scheme is adopted in LS-Dyna software to study machinability and to validate the results obtained from the developed 3D finite element model. A unified numerical and analytical approach to predict flat end milling forces is presented by Mehmet Aydın & Uğur Köklü [12]. They performed numerical simulations of orthogonal cutting of Ti-6Al-4V using Abaqus/Explicit software to analyse the segmented chip formation and validated them with the experimental results.

R. Jalili Saffar [13] et.al simulated the three-dimension cutting forces and tool deflection in the end milling operation based on finite element method. They used 3mm and 6mm uncoated high-speed steel (HSS) endmill to machine mild steel AISI 1045 and validated their simulated results through an experimental study. Erdem Ozturk L [14] investigated the effect of various lead and tilt angles in a full 5 axis ball end milling process. In the work, the effect of tool tip and the surface finish on 12mm ball end mill is analysed for the effect of lead and tilt angles on cutting forces, torque, form errors and stability through, numerical modelling & experimental results.

Prediction of instantaneous cutting forces in 5-axis milling processes with radial cutter runout based on tool motion analysis is presented by Yunwen Sun & Qiang Guo [15]. The work considers an analytical model and five-axis machining experiments on aluminium 2024 to validate the proposed method.

An analytical approach for tool stress and deflection calculations for taper ball end mills in 5 axis machining is presented by Raja Kountanya & Changsheng Guo [16]. In the work, a flute structure with a 6-parameter self-similar motif has been modelled and cutter bending stresses / deflection were analyzed. S.B. Wang et.al [17] presented a cutting force prediction model in a 5-axis milling process considering cutter runout and vibrations. In their work, they numerically modelled the cutter run out and the vibrations effect and verified it with the simulated results. It is by machining with a combination of various lead, tilt angles with the set of process parameters considered in their work. Lee and Altintas [18] applied the geometry and kinematics of the ball end milling process and predicted the cutting forces accurately in tangential, radial, axial directions They measured and validated the fundamental cutting parameters, the yield shear stress, the average frictional coefficient on the rake face and shear angle from a set of orthogonal cutting tests performed at various cutting speeds and feeds.

A mathematical model to measure the edge of the roller nest mill cutter is developed by Kuo and Wu [19]. From the calculated data of the edge, a theoretical value is compared with the measured value and a precise assessment was given for processing the roller nest mill cutter. A generalized mathematical model of helical end mills is presented by Engin and Altintas [20]. They modelled an end mill geometry and evaluated the chip thickness at each cutting point in milling including the structural vibrations of both cutter and workpiece. Xiong Han, Limin Tang [21] presented a cutting force model to predict forces in circular corner milling considering the tool engagement angle / undeformed chip thickness and their calculation in both up and down milling directions. To verify their models, they used carbide end mills with 15.9 mm and 10 mm diameter, to machine titanium alloy Ti-6Al-4V.

Ali Mamedov [22] presented a new force model to analyse the cutter deflection due to the elastic compliance of micro end mill based on predicted cutting forces. They validated the model by machining Ti-6Al-4V using 800 μm diameter two fluted tungsten carbide (WC) micro end mill on a 5-axis milling machine.

From the above research works it can be noticed that the methods have been adopted to improve the machinability, improve tool life, using different cutting tool materials, with 3/5 axis machining scenarios. These are to avoid tool breakages, achieve specified surface finish & tolerance [8-22]. Despite being these works being reported, there is a strong scope where fixed 3+1/3+2 axis can be considered for a FEA & experimental study by analysing the possibility of cutting tool design and other machining parameters reducing tool stresses/strains, forces etc for free form surfaces.

2. Cutting Tool Design and Numerical Model

The work considers standard materials model equation developed by G.R. Johnson, W.H. Cook [23] for the representation of the blank and cutting tool material. As the model equation has been referenced extensively by many researchers [8-22] it is reproduced here for understanding.

$\sigma = [A+B\epsilon^{n}][1+C\ln\epsilon^{*}][1-T^{*m}]$ …Eqn (1);

Where ϵ is the equivalent plastic strain $\epsilon^{*} = \epsilon/\epsilon_0$ is the dimensionless plastic strain rate for reference strain rate for ϵ_0 (1 s^{-1}); and T^* is the homologous temperature. The five material constants are A, *B, n, C, m.* The expression in the first set of brackets gives the stress as a function of strain for $\epsilon^*= 1.0$ and $T^* = 0$. The expressions in the second and third sets of brackets represent the effects of strain rate and temperature, respectively. The JC model parameters of Ti-6Al-4V is A = 862 (MPa), B = 331 (MPa), n = 0.34, C = 0.12, and m = 0.8. The damage of a FEA element is given by $D = \sum(\Delta\epsilon / \epsilon^{f})$. ϵ^{f} is the equivalent strain to fracture under current conditions and strain rate, temperature, pressure, and equivalent stress. Fracture is then allowed to occur when $D = 1.0$. The JC failure model [26] was applied as an initial damage criterion, which is formulated by Eq (2). It contains five failure parameters Di (i = 1, 2, 3, 4, 5), which represent initial failure strain, exponential factor, triaxiality factor, strain rate factor and temperature factor, respectively. The JC failure model parameters of Ti-6Al-4V [23] are given as D1=−0.09; D2= 0.25; D3=−0.5; D4=0.014; D5=3.87.

Equivalent plastic strain = $\epsilon^{f} = [D1+D2\exp D3\,\sigma^{*})][1+D4\ln\epsilon^{*}][1+D5\,T^{*}]$ …Eqn (2);

Where $\sigma^* = \sigma_m / \sigma^{\wedge}$, where σ_m is the average of the 3 normal stresses and $\sigma^{\wedge}$ is the von Mises equivalent stress. The dimensionless strain rate, ϵ^*, and homologous temperature, T^*, are identical to those used in the strength model of eqn (1). The five constants are *D1 . . . D5.* The expression in the first set of brackets follows the form presented by Hancock and Mackenzie [24]. It essentially says that the strain to fracture decreases as the hydrostatic tension, σ_m increases. The expression in the second set of brackets represents the effect of strain rate, and that in the third set of brackets represents the effect of temperature. For high values of hydrostatic tension ($\sigma^* > 1.5$) a different relationship is used; it will be presented later.

3. Machining Scenario and Mathematical Theory adopted for FEA simulation

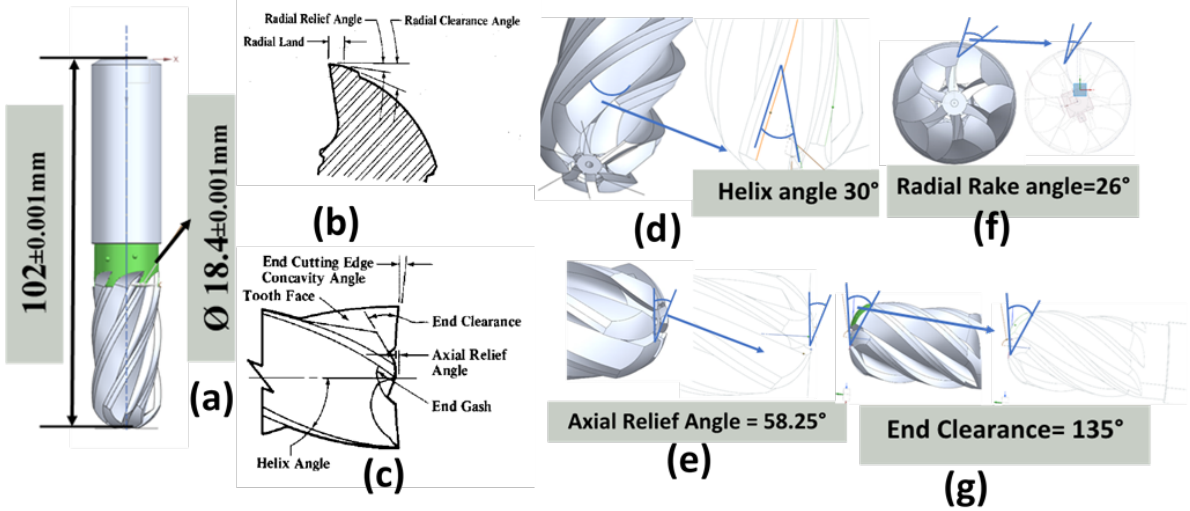

Fig. 3. An 18.4mm ball end mill with standard cutting tool nomenclature and associated numerical values

To address the above problem and to discuss the cutting tool engagement while machining, a ball end mill with 6 fluted Ø18.4mm diameter is considered (Fig. 3(a)). The Fig's. 3 (b) & (c) explains the standard nomenclature of various dimensional parameters associated with the end mill. Fig's. 3(d)-(g)) are presented with the actual values corresponding to the to the Ø18.4mm diameter ball end mill. Using this end mill, various 3+1 & 3+2 tool orientations are applied in the blank (110x100x100mm) as shown in Fig. 4. This is with (i) tilt angles of 5°, 10°, 15° and 20° for fixed 3+1 axis and (ii) tilt angle of 10° with lead angles of 5°, 10° and 15° for fixed 3+2 axis. Based on these conditions, the standard cutting tool-based mathematical model considered by many researchers is adopted for FEA analysis and has been reproduced for understanding below [18, 14, 17, 20]. Ball end mill flutes are treated as combination of series of oblique cutting-edge segments. An oblique cutting geometry based on the thin shear zone model [18] is shown in

Fig.5 where the chip velocity V_c is inclined at an acute angle 'i' to the plane P_n normal to cutting edge. The tangential, axial and radial force component equations are given below:

$$F_t = \frac{(\tau .b .t .cos(\beta_n - \alpha_n) + tan\eta_c.sin\beta_n.tan\, i)}{(c\,.\ sin\varphi_n)} \quad \ldots\text{Eqn (3);}$$

$$F_r = \frac{(\tau .b .t .sin(\beta_n - \alpha_n))}{(cosi .c .sin\varphi_n)} \quad \ldots\text{Eqn (4);}$$

$$F_a = \frac{(\tau .b .t .cos(\beta_n - \alpha_n) .tani - tan\eta_c.sin\beta_n)}{(c .sin\varphi_n)} \quad \ldots\text{Eqn (5);}$$

$$c = (cos^2(\varphi_n + \beta_n - \alpha_n) + tan^2\eta_c sin^2\beta_n)^{1/2}; \quad \ldots\text{Eqn (6);}$$

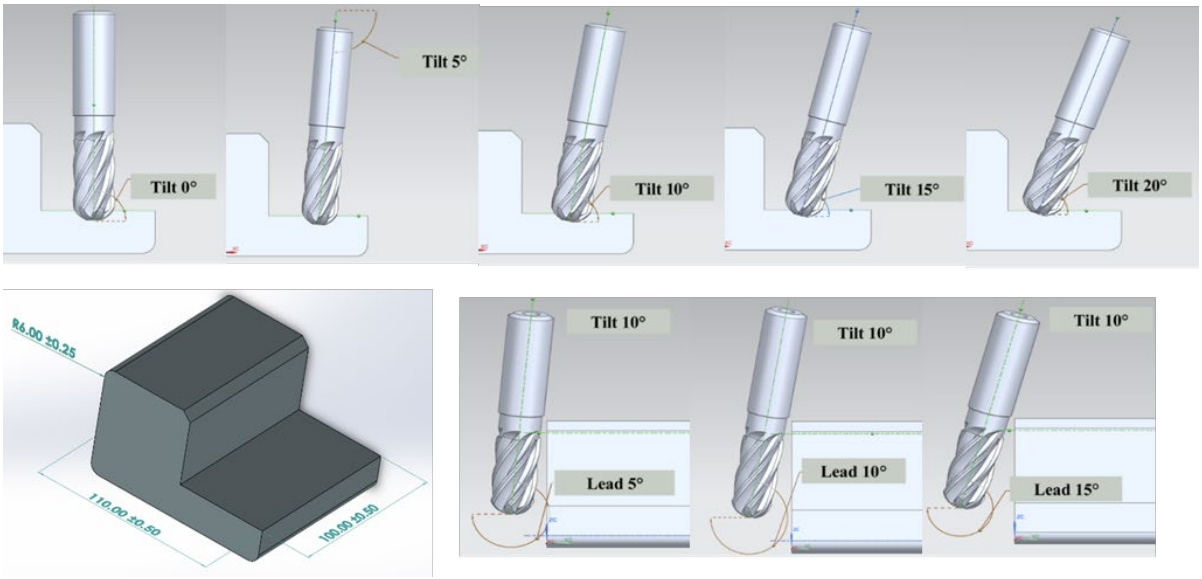

Fig. 4. Various 3+1 & 3+2 tool orientations (tilt and lead angles) considered in the work

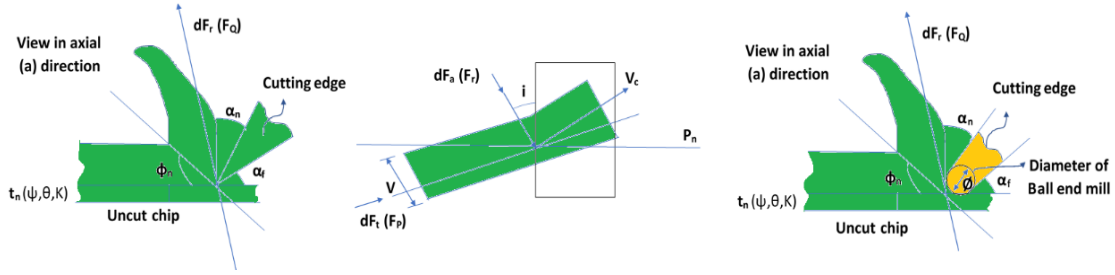

Fig. 5. Oblique cutting geometry

F_t, F_r, F_a are the tangential, radial and axial forces acting on the oblique cutting-edge segment respectively. The normal friction angle, β_n, is defined as

$$tan\beta_n = tan\beta\, cos\eta_c \quad \text{and} \quad tan\varphi_n = \frac{(r_t cos\alpha_n)}{(1 - r_t sin\alpha_n)} \quad \ldots\text{Eqn (7);}$$

where β is the average friction angle at the rake face of an orthogonal cut and η_c is the chip flow angle (the angle between a perpendicular to cutting edge and the direction of chip flow over rake face, as measured in the of tool face).The normal rake angle is constant and set during cutter grinding as shown in Fig2. The normal shear angle , φ_n, is obtained from the cutting ratio

$\tan\varphi_n = r_t \cos\alpha_n / 1 - r_t \sin\alpha_n$ …Eqn (8); $0 < \alpha_n < 20^o (for\ minimum\ friction\ angle)$; $\beta = 19.1 + 0.29\alpha_n$

where 'r_t' is the chip thickness ratio in oblique cutting and is related to orthogonal parameter 'r' by

$$r_t = \frac{(r\, cos\eta_c)}{(cos\, i)}\ ; \ldots\text{Eqn (9);}$$

With the above cutting tool equations (Eqn's 3-9), the values of standard dimensional parametes [18] are considered and first theoretical cutting tool forces for 9mm and 18.4mm ball end mills are calculated. Here the width of cut is taken to be equivalent to match the diameter of tool with assumptions as applicable to the present problem. Owing to page restricitons only a part of the table is presented here.

Table -1 Theoretical calculation of cutting tool forces based on adotped standard formulas

S.No	α_n	β	β_n	η_c	i	r_t	Φ_n	t	b	τ	c	F_t	F_r	F_a	F_t
	Normal rake angle	Friction angle on the rake face.	Normal friction angles in oblique cutting	Chip flow angle	Local helix angle	Cutting chip ratio	Normal shear angles in oblique cutting	Uncut chip thickness	Width of cut	Shear stress at the shear plane	In Equation	Tangential force (N)	Radial force (N)	Axial force (N)	Total force (N)
	deg°	deg°	deg°	deg°	deg°		deg°	mm	mm	MPa		N	N	N	N
1	4.00	20.26	20.19	5.00	5.00	0.50	27.47	5.00	9.00	9.00	0.72	1164	339	102	1217
2	6.00	20.84	20.65	8.00	8.00	0.50	27.90	3.00	18.40	4.00	0.74	618	163	87	645
3	8.00	21.42	21.23	8.00	8.00	0.50	28.31	3.00	18.40	4.00	0.75	603	143	85	626
4	10.00	22.00	21.89	6.00	6.00	0.50	28.71	5.00	9.00	8.00	0.76	964	204	101	990
5	12.00	22.58	22.27	10.00	10.00	0.50	29.09	5.00	9.00	8.00	0.78	937	172	165	967
6	16.00	23.74	23.42	10.00	10.00	0.50	29.77	5.00	18.40	3.00	0.80	688	91	121	704

4. Setting and Meshing for FEA Simulation

Based on the above plan, CAD models of both blank / cutting tool are modelled and imported to the Explicit Dynamics ANSYS research simulation environment. The blank and cutting tool are assigned with Ti-6Al-4V and WC by fixing the side / base faces to depict the actual fixation of blank in a CNC milling machine. The cutting speed and feed rate per tooth is taken as 450m/min and 0.5 mm/tooth. Standard temperature of 22°C is taken as the machining environment with dry machining conditions with friction coefficient and the dynamic coefficient as 0.4 / 0.1. With a meshing resolution of 7 and default meshing size of max 2mm, 73,432 nodes has been generated with 121,876 elements (Fig.6). The simulation is performed with the following settings (i) a maximum of 1.75e+05 cycles (ii) geometric strain limit to 0.5 (iii) the tool with a remote displacement of 180mm in the Y direction and (iv) with a Z degree rotation of 360°. The simulation completed with approximately 410- 420 minutes (6-7 hours) for all orientations and the following parameters are calculated (i) the stresses ($\sigma_{max/min\text{-}principal}$) (ii) strains ($\varepsilon_{max/min(elastic\ and\ equivalent\ plastic/elastic)}$) and (iii) forces in F_x, F_y, F_z and F_{total} directions. Owing to page restrictions only the $\sigma_{max\text{-}principal}$ and $\varepsilon_{max\text{-}max\text{-}principal\text{-}elastic}$ and total forces are presented. As adopted by many researchers [8-23] the materials model developed by G.R. Johnson, W.H. Cook [23] and the standard cutting tool-based mathematical model is adopted for this FEA analysis [15-20].

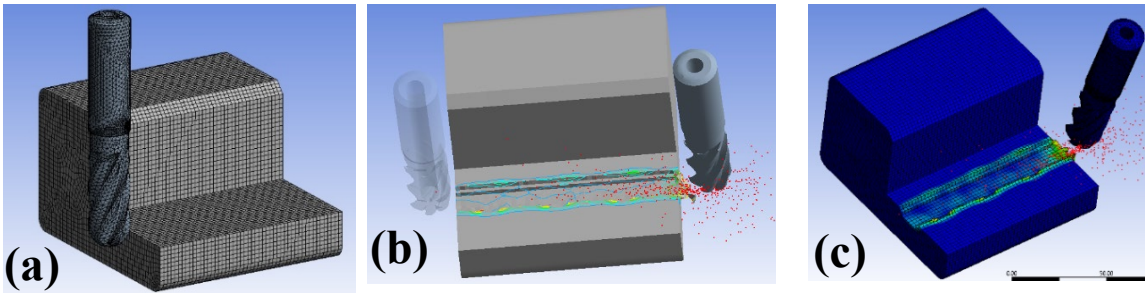

Fig. 6. FEA setup showing (a) meshed model (b) initial / final movement of cutting tool and (c) final simulation

Comparison and Effect of 3+1 orientation : Analysis of Maximum Principal Elastic Strain: The plot shown in Fig. 7(a) represents the maximum principal elastic strain recorded at 16-20 cutting points considering 3+1 orientations. From the plot, higher values of elastic strains can be noticed at Point 4 (P4) and Point 5 (P5) corresponding to the times of 7.5e-5s and 1e-4s. The highest value of 0.106mm/mm corresponding to 64870 cycle is recorded for tilt angle of 15° is probed and is shown in (Fig. 7(b) (highlighted green). A closer analysis at the point of occurrence with Iso surfaces (Fig. 7(c)) with an undeformed model shows that the maximum principal elastic strain (highlighted green) is occurring internally at the at the centre of the tool (Fig.7(d)). For the tilt angles of 0, 10, a similar trend can be seen which is reduced / normalized to values with minimal variation along the whole machining process. Tilt angle of 20° shows slight variation at this point but normalises similar to trend seen in other tilt angles until the end of the cutting process. At all the tilt angles a higher value of maximum principal elastic strain can be noticed at the starting Point P2 until P4- P5, before being normalized gradually. The reason is as this the start of the cutting process, heavy strain will be created up by the cutting tool to cut the material and it is natural to see higher values at the initial point. Tilt angles 10 ° &, 15° follow a closer strain behaviour and converging until Point 10 (P10) with less variation before diverging until the end of the machining process. Tilt angle 0° shows slight variation after P4 & P5 until the end of the machining

process. This is owing to the full engagement of the cutting tool faces and the ability to maintain a constant cutting process at all locations. On the other side, tilt angle of 5° shows similar trend like other tilt angles until Point 10 (P10) before varying drastically from a lower value of 2.871e-2 to a higher value of 9.02e-02 at Point 11 (P11). To analyse this point, a closer analysis is performed to find the exact location of this value in the tool. With the present node's limitations, the exact location is difficult to be probed (Fig.8(a)) and hence another simulation is performed with a mesh element size to 0.5. It is located at an internal point inside the cutting tool (Fig. 8(b)). It can also be seen that the average of the maximum and minimum strain lies close to the zero and hence the machining with the present condition is safe to proceed.

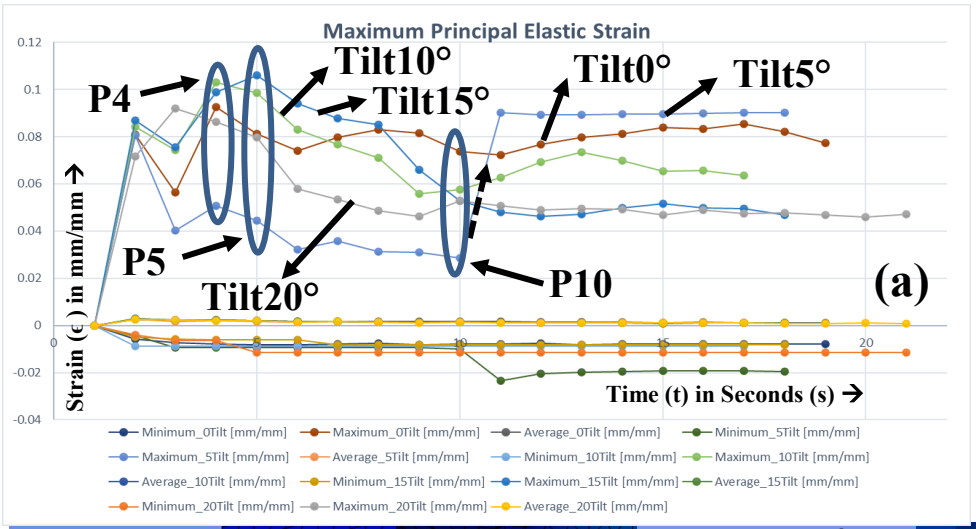

	Time [s]
1	1.18E-38
2	2.50E-05
3	5.00E-05
4	7.50E-05
5	1.00E-04
6	1.25E-04
7	1.50E-04
8	1.75E-04
9	2.00E-04
10	2.25E-04
11	2.50E-04
12	2.75E-04
13	3.00E-04
14	3.25E-04
15	3.50E-04
16	3.75E-04
17	4.00E-04
18	4.25E-04
19	4.27E-04

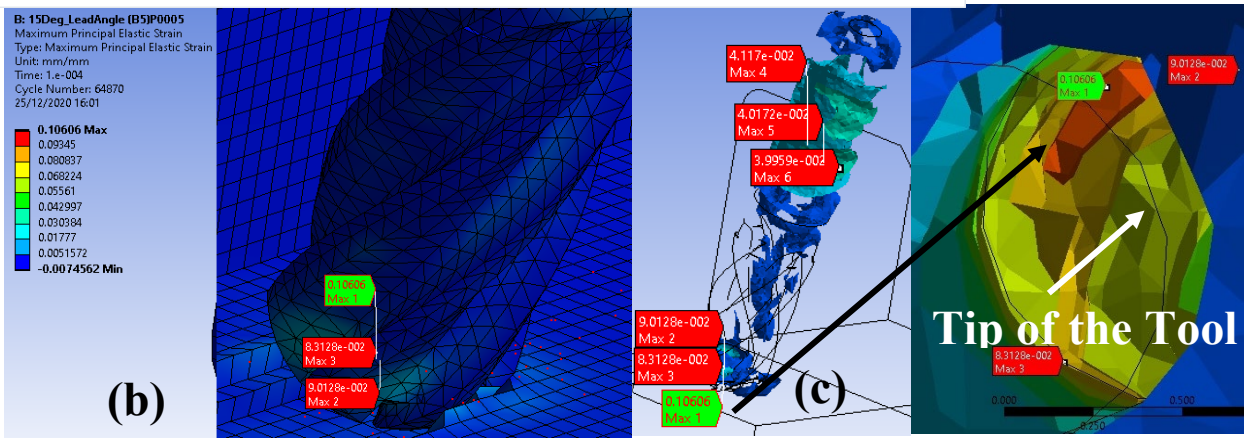

Fig. 7. (a) Plotted simulation results of maximum principal elastic strain obtained in all 3+1 axis orientations (b) Highest value probed at point P5 for tilt angle 15° (c) Iso surface showing the exact location in the tool at point P5 for tilt angle 15°

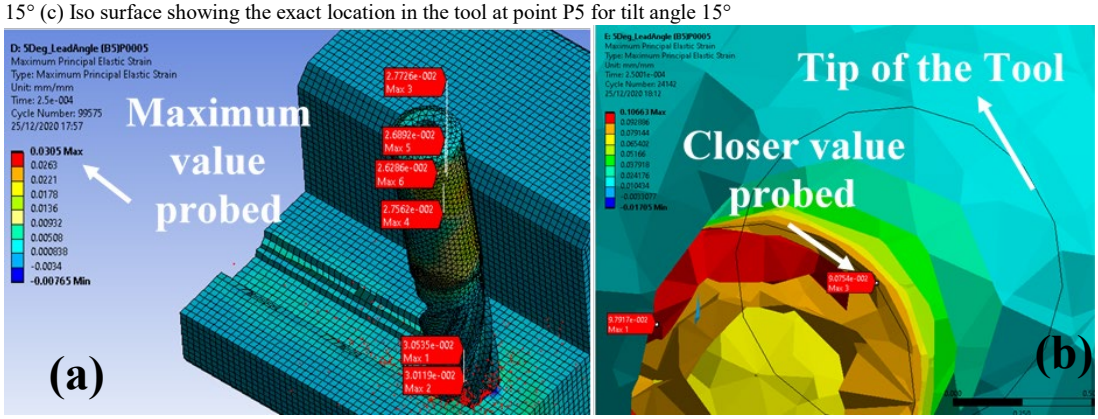

Fig. 8. (a) Limitations with lower mesh size for the maximum value probed value at point P11 for tilt angle 5° (b) Closer value probed from the simulation with higher mesh size at point P11 for tilt angle 5°

Comparison and Effect of 3+1 orientation : Analysis of Maximum Principal Stress: The output from the simulation for maximum principal stress is presented in Fig. 9. At all the angles except 5° the maximum principal stress pattern follows the same trend. i.e. with a higher value at the tool entry in cutting followed by slight reduction then higher values before being normalized until the end of machining. It can be noticed that when the tilt angle is increased from 0° to 20° the stresses involved with the machining process are reduced. Except 5° shows a much lower value than the others and a thorough investigation on the effect on helix angle and rake angle is needed to further analyse this variation. The lesser stresses in other tilt angles are owing to the less engagement of the ball mill face where the relief angle reduce the stresses created while milling. The highest stress occurred at the Point 4 (P4) for Tilt angle 10° corresponding to 7.5e-5 with the value of 5.77e+4 MPa (highlighted green) has been probed and shown in Fig.10 (a) and (b).

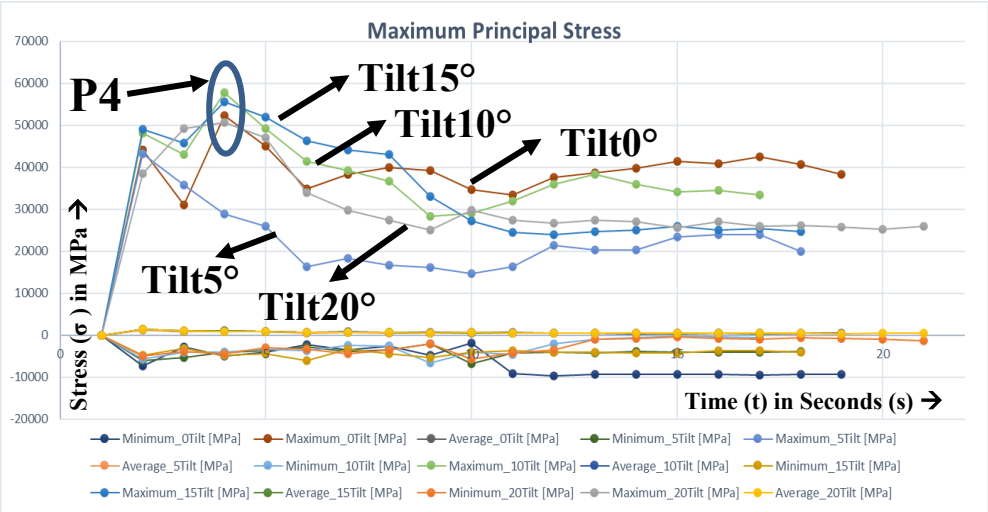

	Time [s]
1	1.18E-38
2	2.50E-05
3	5.00E-05
4	7.50E-05
5	1.00E-04
6	1.25E-04
7	1.50E-04
8	1.75E-04
9	2.00E-04
10	2.25E-04
11	2.50E-04
12	2.75E-04
13	3.00E-04
14	3.25E-04
15	3.50E-04
16	3.75E-04
17	4.00E-04
18	4.21E-04

Fig. 9. Plotted simulation results of maximum principal stress obtained in all 3+1 axis orientations

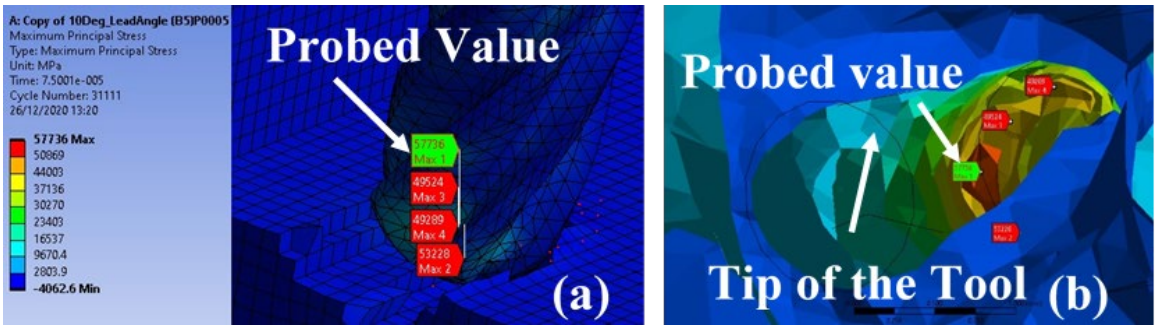

Fig. 10. Maximum principal stress of (a) The highest value probed at point P4 for tilt angle 10° (b) Iso surface showing the exact location in the tool at point P4 for tilt angle 10°

Comparison and Effect of 3+1 orientation : Analysis of Cutting Forces : The cutting forces involved with the machining process is plotted and given in **Fig. 11.** It highlights the axial (Fz), radial (Fy), tangential (Fx) and the total forces involved while machining with different tilt angles. In the plot, the forces along radial direction (Fy) is recorded higher at the initial instance of the cutting process as this corresponds to the cutting feed direction along Y axis. The tangential (Fx) and the axial (Fz) forces associated with the chip flow and spindle rotation during the cutting process are lower at various recorded points validating the suitability of selected process parameters. In all the considered orientations, the variations with the forces in all the three directions comes closer to each other irrespective of the tilt angles associated with them. The total force, which is the square root of the summation of individual squares Fx, Fy and Fz, remains high with 638.4 N at a tilt angle of 5° showing minor variations with other tilt angles. i.e., as per milling theory, the approach angle associated with the rake angle will have lesser effect on the cutting forces but remains high in HSM owing to the material properties of the cutting tool and blank. The Table 1 is compared with the simulated results obtained for a 0° tilt angle and it can be traced to the result at Point 5 (P5). It should be noted the values in the table corresponds to 0° tilt angle at normal conditions and with standard values.

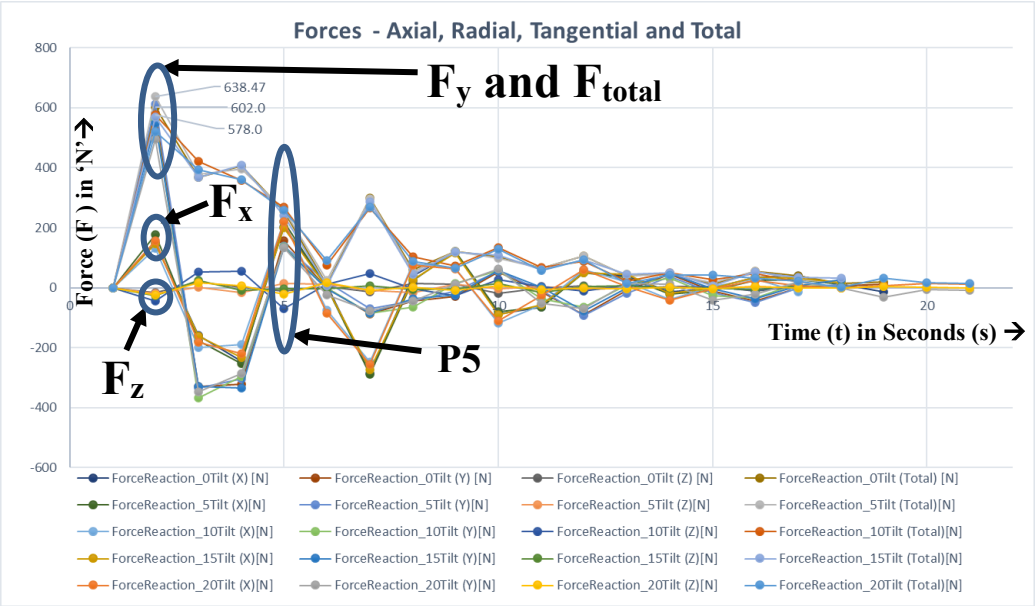

	Time [s]
1	1.18E-38
2	2.50E-05
3	5.00E-05
4	7.50E-05
5	1.00E-04
6	1.25E-04
7	1.50E-04
8	1.75E-04
9	2.00E-04
10	2.25E-04
11	2.50E-04
12	2.75E-04
13	3.00E-04
14	3.25E-04
15	3.50E-04
16	3.75E-04
17	4.00E-04
18	4.25E-04
19	4.27E-04

Fig. 11. Plotted simulation results of axial, radial, tangential and total forces obtained in all 3+1 axis orientations

Comparison and Effect of 3+2 orientation : Analysis of Maximum Principal Elastic strain : The plots corresponding to the maximum principal elastic stain is given in Fig.12. Similar to the trend with the tilt angles, the initial Point (P2) can be noticed at all 3+2 orientations. The highest value 0.1015 mm/mm seen for Tilt 10°/Lead 10° is probed and found to be located internally (highlighted green) at the top side of the tool (Fig. 13(a)-(c)). Further the values reduce in the next two points and becomes gradually normalises with less variation until the end of machining process.

Comparison and Effect of 3+2 orientation : Analysis of Maximum Principal Stress : The maximum principal stress seen from the plot in Fig.14 corresponding the same point show a similar trend with variation in values lowering with the lead angles of 10°, 15° and 5°. For all angles at Point 3 (P3) the stress value drops before being increased at Point 4 (P4). After this point the value slightly varies before it normalises until the end of machining. It can be noticed that the combination of tilt 10°and lead angles of 10°, 15° and 5° attain a higher value of 5.30E+04, 5.06E+04 MPa & 4.71E+04 MPa. In both the plots given in Fig 11 (a) and (b) the maximum average value recorded are 1.73E+03MPa, 1.68E+03MPa, 1.42E+03 MPa for lead angles of 10°, 15° and 5°.

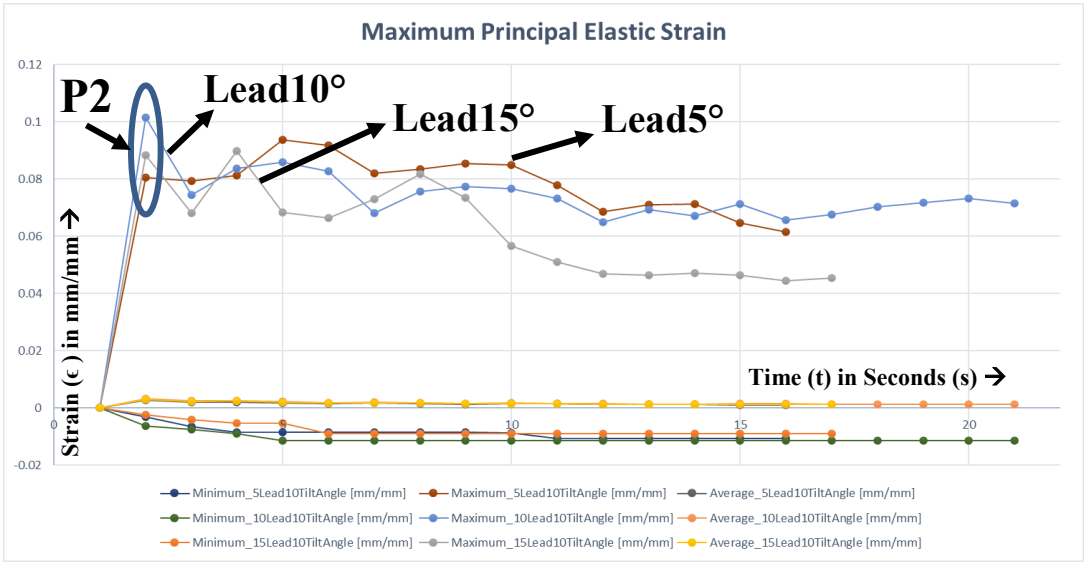

Fig. 12. Plotted simulation results of maximum principal elastic strain obtained in all 3+2 axis orientations

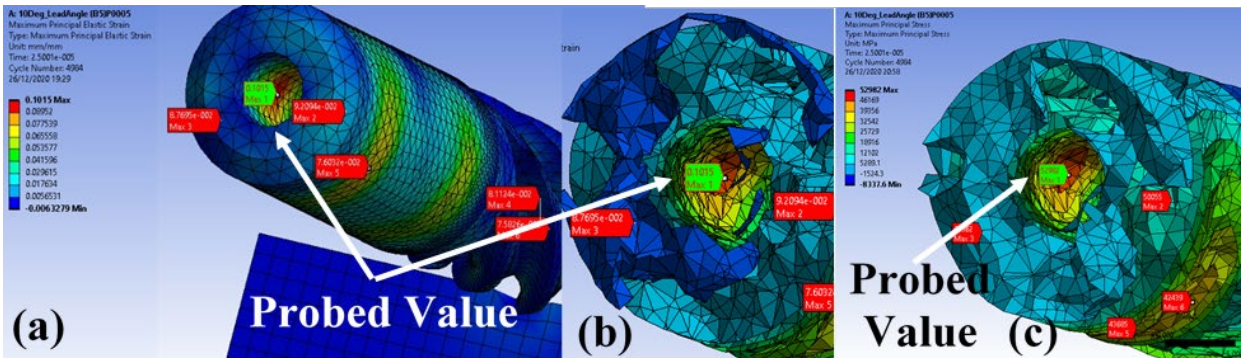

Fig. 13. (a) Highest maximum principal elastic strain value probed at point (P2) for Tilt 10°/Lead 10° (b) Iso surface of maximum principal elastic strain showing exact location in the tool at point (P4) for Tilt 10°/Lead 10° and (c) Iso surface of maximum principal stress showing highest value location in the tool at point (P4) for Tilt 10°/Lead 10°.

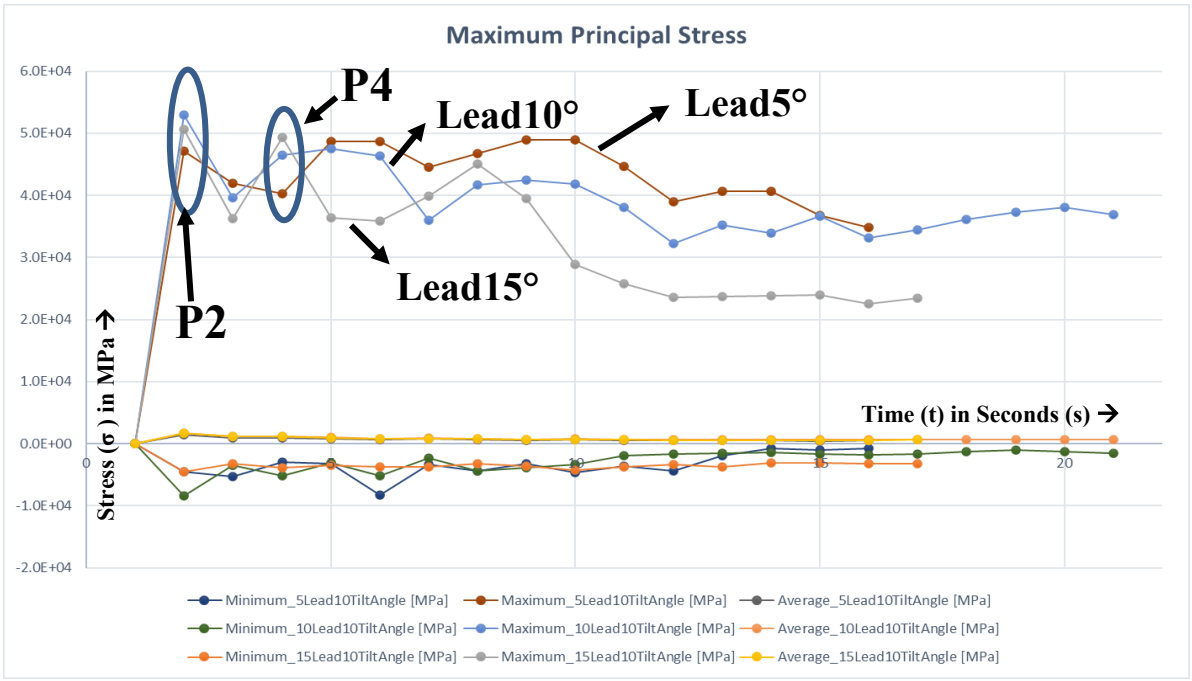

Fig. 14. Plotted simulation results of maximum principal stress obtained in all 3+2 axis orientations

Comparison and Effect of 3+2 orientation : Analysis of Cutting Forces : The plot shown in the Fig. 15 are the results obtained from the simulation for 3+2 orientation in the the axial (Fz), radial (Fy), tangential (Fx) directions. Similar to the results obtained from the tilt angles for 3+1 orientations the tangential force (Fx) stays with a lower value when compared with the radial force (Fy). The axial force (Fz) remains closer to the tangential force (Fx) but varies constantly between positive and negative values throughout the cutting process. It can also be noticed the total force corresponding to Tilt 10°/Lead 10° is 741.3N, Tilt 10°/Lead 15° is 608.5 N and Tilt 10°/Lead 5° is 583.7 N. This clearly shows that the forces are increased with the increase in lead angle from 5° to 10° but reduced when further increased to 15°. The Table 1 is compared with the simulated results obtained for a 0° tilt angle and it can be probed to the result at Point 5 (P5) similar to with 3+1 orientations. From both orientations, it is clear that the forces are relatively higher and hence further investigation into the effect of lead angle, the tilt angle with the rake, relief and the helix angles are needed. This is by varying the FEA meshing, varying the geometric strain limit and other parameters by validating through experimental results. Fig. 16, presented with the total forces (F_{total}) for both orientations highlighting, 5° tilt angle of 638.5 N and Tilt 10°/Lead 10° of 743.3 N along with other values.

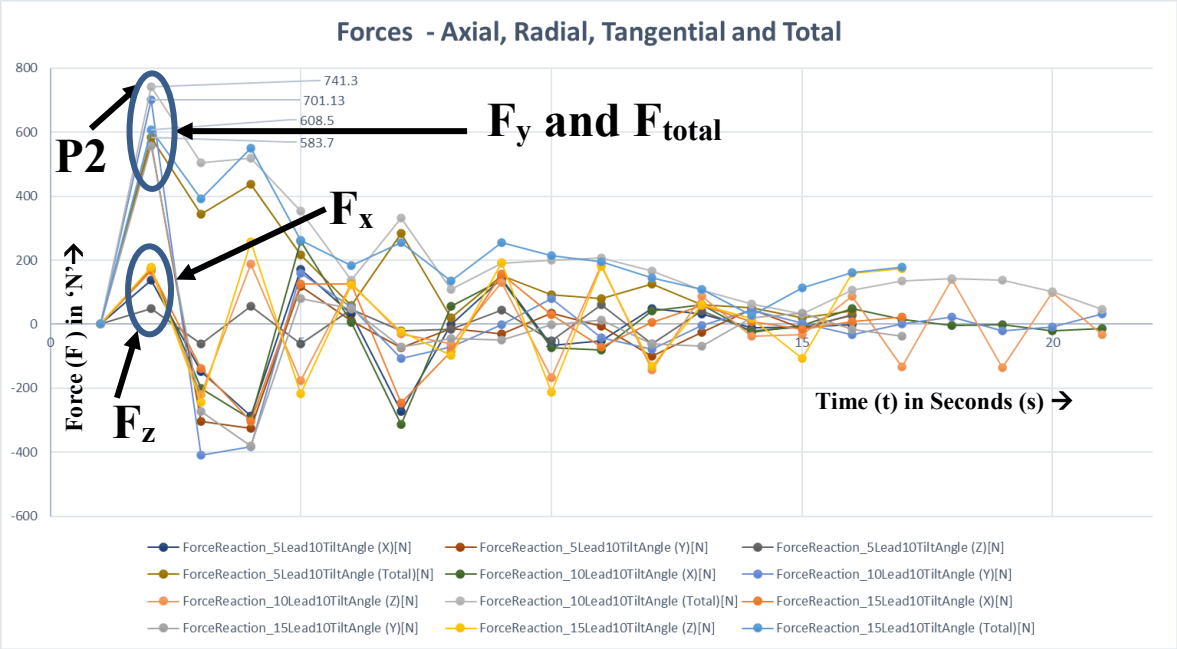

Fig. 15. Plotted simulation results of axial, radial, tangential and total forces obtained in all 3+2 axis orientations

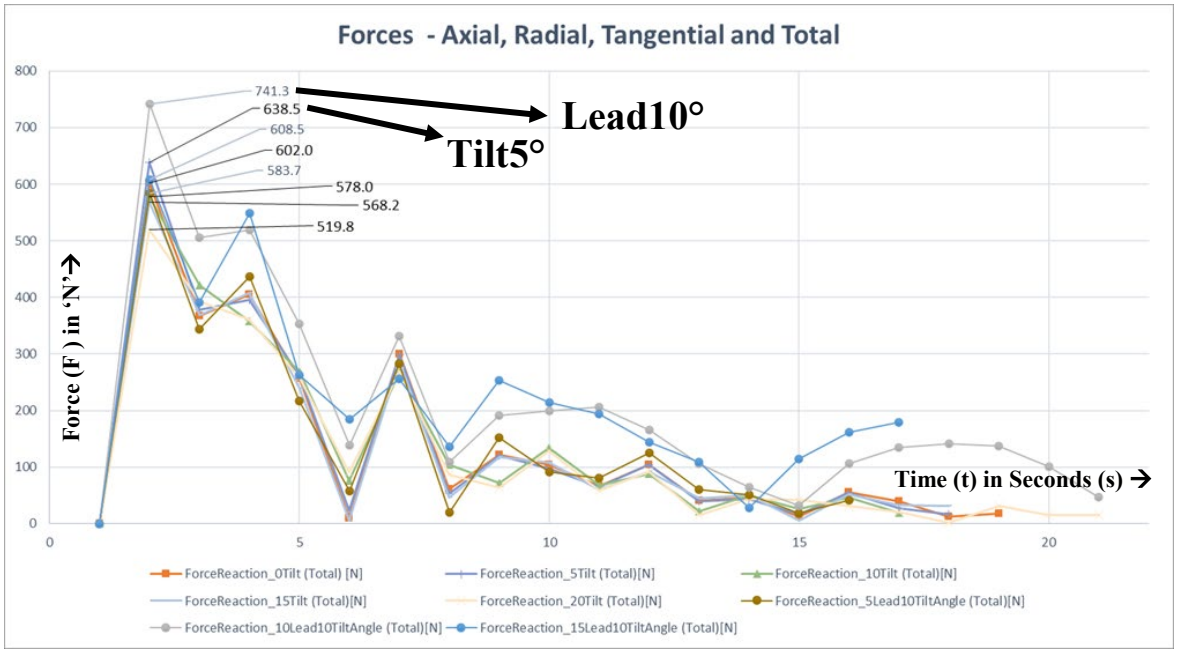

Fig. 16. Combined plot of total force (F_{total}) for both 3+1 & 3+2 axis orientations

5. Experimental Setup and validation.

In order to experimentally verify the preliminary FEA study, setup as shown in the Fig. 17 is adopted to machine Ti-6Al-4V in a CNC milling machine. The axial, radial and tangential forces are measured with 9257B KISTLER stationary piezoelectric dynamometer. The machining is conducted with a series of 1mm-18.4mm ball end mills. First ball end mill with Ø9mm in diameter is verified and the recorded tool forces are shown in Fig. 18 in relation to the trial 1 and trial 6. Table 2 is presented with the results of the forces in all the directions and can be related to the theoretical forces given in the Table 1. It should be noted that the work is ongoing on different cutting tool and blank materials. The first set of preliminary results with considered feeds and speeds are presented in Table 2.

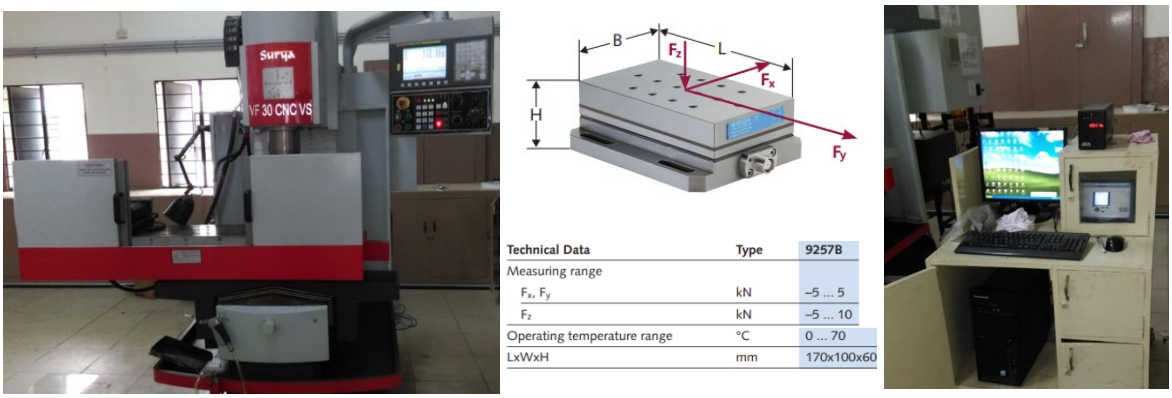

Fig. 17. CNC milling machine with 9257B KISTLER stationary piezoelectric dynamometer and Dynoware software

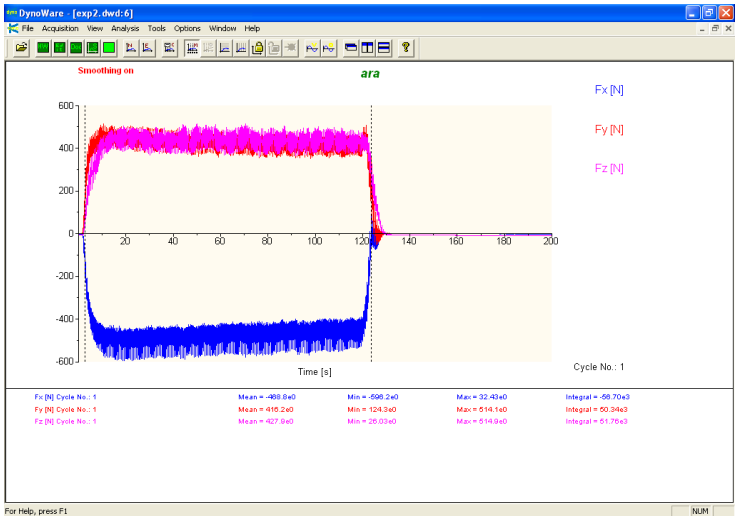

Fig. 18. Cutting Tool Forces - Output results for Trial 1 from Dynoware software

Table 2. Force analysis recorded for end mill tool 9mm

S.No	Spindle speed (rpm)	Feed (f_n) (mm/min)	Axial / Radial Depth of Cut (mm)	Tangential (F_x) (N)	Radial (F_y) (N)	Axial (F_z) (N)	Total (N)
Trial 1	65	8.45	1.2	-468.8	416.2	427.9	759.0
Trial 2	105	42	1.6	-516.7	657.1	374.5	915.9
Trial 3	185	111	2	503.9	665	270.6	877.1
Trial 4	280	224	2.5	-663.6	-879	359.8	1158.6
Trial 5	405	405	3	817.9	1.0e3	448.3	932.7

6. Conclusions & Scope for Future Work

In this article, a study based on FEA simulation study is presented for fixed 3+1 / 3+2 axis orientations by considering different tilt & lead angles. It has been conducted in ANSYS software using specified cutting tool design and process parameters by verifying the machining of Ti-6Al-4V with tungsten carbide ball end mills. At each tilt / lead angles the maximum principal elastic strain, principal stress, total forces are recorded at 16-20 cutting points in the blank. From the results, it is observed that the average values of maximum principal elastic strain and principal stress are closer to zero. This indicates that the damage to the life of the tool will be lesser for the specified cutting tool design and process parameters. It is also noticed that when the meshing size on these simulations are increased, the results of exact location and point can be probed easily. At present the meshing is limited to a meshing size of max 2mm with elastic strain limit / coefficient of friction as 0.5 / 0.4. Any changes to these limits and varying the cutting tool design parameters will help to increase and analyse the simulation and a further investigation is needed. The

present work is ongoing and parallely the results of FEA simulation for the cutting tool design parameters are improved and being validated through experimental trials in a CNC milling machine.

References

[1] Peter Smid, CNC Programming Handbook, Industrial Press, Inc, 3 Rev Ed Edition, 2008.
[2] Milling with Sinumerik - 5 axis machining Manual, Siemens, Sinumerik Documentation, 05/2009.
[3] Siemens NX, CAD/CAM software, 2020.
[4] 3+2 Vs. 5-axis: What's the Difference? Okuma, 2019, Manufacturing Tomorrow, Online Trade Magazine, https://www.manufacturingtomorrow.com/article/2019/09/32-vs-5-axis-whats-the-difference/14074.
[5] A.Arivazhagan, Toolpath algorithm for free form irregular contoured walls / surfaces with internal deflecting connections, Materials Today: Proceedings 22 (2020) 3037–3047.
[6] Ravi Kumar, Surya Prakash Singh, Kuldeep Lamba, Sustainable robust layout using Big Data approach: A key towards industry 4.0, Journal of Cleaner Production 204 (2018) 643-659.
[7] Roy Woodhead, Paul Stephenson, Denise Morrey, Digital construction: From point solutions to IoT ecosystem, Automation in Construction 93 (2018) 35–46.
[8] Thanongsak Thepsonthi, Tugrul Özel, 3-D finite element process simulation of micro-end milling Ti-6Al-4Vtitanium alloy: Experimental validations on chip flow and tool wear, Journal of Materials Processing Technology, 221 (2015), 128–145.
[9] Puneet Tandon, Md. Rajik Khan, Three dimensional modeling and finite element simulation of a generic end mill, Computer-Aided Design, 41 (2009) 106-114.
[10] Xiaoliang Jin, Yusuf Altintas, Prediction of micro-milling forces with finite element method, Journal of Materials Processing Technology 212 (2012) 542– 552.
[11] A. Maurel-Pantel, M. Fontaine , S. Thibaud , J.C. Gelin, 3D FEM simulations of shoulder milling operations on a 304L stainless steel, Simulation Modelling Practice and Theory 22 (2012) 13–27
[12] Mehmet Aydın, Uğur Köklü, Analysis of flat end milling forces considering chip formation process in high-speed cutting of Ti-6Al-4V titanium alloy, Simulation Modelling Practice and Theory 100 (2020) 102039.
[13] R. Jalili Saffar, M.R. Razfar, O. Zarei, E. Ghassemieh, Simulation of three-dimension cutting force and tool deflection in the end milling operation based on finite element method, Simulation Modelling Practice and Theory 16 (2008) 1677–1688.
[14] Erdem Ozturk L, Taner Tunc, Erhan Budak, Investigation of lead and tilt angle effects in 5-axis ball-end milling processes, International Journal of Machine Tools & Manufacture 49 (2009), 1053–1062
[15] Yunwen Sun, Qiang Guo, Numerical simulation and prediction of cutting forces in five-axis milling processes with cutter run-out, International Journal of Machine Tools & Manufacture, 51 (2011), 806–815.
[16] Raja Kountanya, Changsheng Guo, On the geometric and stress modeling of taper ball end mills, CIRP Annals - Manufacturing Technology 63 (2014), 117–120.
[17] S.B. Wang, L.Geng, Y.F.Zhang, K.Liu, T.E.Ng, Cutting force prediction for five-axis ball-end milling considering cutter vibrations and run-out, International Journal of Mechanical Sciences 96-97, (2015), 206–215.
[18] P. Lee, Y. Altintas, Prediction of Ball-End Milling Forces from Orthogonal Cutting Data, International Journal of Machine Tools & Manufacture, Vol. 36, No. 9. pp. 1059-1072, 1996.
[19] H.Kuo and L.J.Wu(2001) "A study on the evaluation of a model of the precise outside of the roller mill cutter" ,Journal of Materials Processing Technology,pp.178-182.
[20] S.Engin and Y.Altintas (2001), Mechanics and dynamics of general milling cutter, Part I: helical end mills, International Journal Machine Tools Manufacturing, pp.2195-2212.
[21] Xiong Han, Limin Tang, Precise prediction of forces in milling circular corners, International Journal of Machine Tools & Manufacture, 88 (2015), 184–193.
[22] Ali Mamedov, S. Ehsan Layegh K, Ismail Lazoglu, Instantaneous tool deflection model for micro milling, International Journal of Advanced Manufacturing Technology (2015) 79:769–777, DOI 10.1007/s00170-015-6877-9.
[23] G.R. Johnson, W.H. Cook, A constitutive model and data for metals subjected to large strains, high strain rates and high temperatures, Proceedings of the 7th International Symposium on Ballistics, The Hague, The Netherlands, 1983, pp. 541–547.
[24] J. W. Hancock and a. C. Mackenzie, On the Mechanisms of Ductile Failure In High-Strength Steels Subjected To Multi-Axial Stress-States, J. Mech. Phys. Solids, 1976, Vol. 24, pp. 147 to 169. Pergamon Press.